JOURNAL OF PROPULSION AND POWER
Vol. 25, No. 3, May–June 2009

Mixing and Combustion Characteristics of Kerosene in a Model Supersonic Combustor

K. Kumaran* and V. Babu†
Indian Institute of Technology, Madras 600 036, India

DOI: 10.2514/1.40140

In this numerical study, supersonic combustion of kerosene in three model combustor configurations is investigated. To this end, 3-D, compressible, turbulent, nonreacting, and reacting flow calculations with a single step chemistry model have been carried out. For the nonreacting flow calculations, the droplet diameter distribution at different axial locations, variation of the Sauter mean diameter, and the mixing efficiency for three injection pressures are presented and discussed. In addition, the effect of turbulent dispersion on the mixing efficiency is studied using a stochastic model in conjunction with the two-equation shear stress transport k-ω turbulence model. For the reacting flow calculations, contours of heat release and axial velocity at several axial locations are used to identify regions of heat release inside the combustor. Combustion efficiency predicted by the present results is compared with earlier predictions for all the combustor models. Furthermore, the predicted variation of static pressure along the combustor top wall is compared with experimental data reported in the literature. Calculations show that the penetration and spreading of the fuel increases with an increase in the injection pressure. Predicted values of the combustion efficiency are more realistic when the spray model is used for modelling the injection of the fuel. The importance of the mixing process, especially for a liquid fuel such as kerosene, on the prediction of heat release is discussed in detail.

I. Introduction

RENEWED interest in hypersonic flights has motivated research efforts toward developing a supersonic combustion ramjet (scramjet) engine. Supersonic combustion is the key enabling technology for sustained hypersonic flights. In scramjet engines, the combustor length is typically of the order of 1 m and the residence time of the fuel–air mixture is of the order of a millisecond (for flight Mach numbers $M = 6$ to 8). Beyond $M = 10$, fuel has to be injected in the mainstream direction as the momentum of the fuel jet considerably augments the overall thrust. However, at lower hypersonic regimes ($M < 8$), transverse fuel injection has proven to have a higher penetration into the core flow. Nevertheless, because the fuel is injected into a supersonic flow, the mixing process is highly inefficient, especially in the case of a liquid fuel such as kerosene, which has to atomize and evaporate before mixing. This, in turn, demands longer residence times for better mixing at higher velocities and, hence, a longer combustor. However, a short combustor is desirable from the consideration of the thrust-to-drag ratio of an engine, because it is approximately proportionate to the ratio of the combustor diameter to the length [1]. Moreover, in compact engines, the combustor diameter is usually small, and so the length has to be scaled accordingly. All these constraints demand a better mixing strategy at supersonic speeds within a short combustor length.

Over the years several fuel-injection strategies, such as strut, wall, and ramp, and several flame-holding strategies, such as rearward-facing step and cavities of different configurations, have been proposed and extensively studied. Though efficient mixing is the objective in all these injection strategies, the total pressure loss and drag (resulting in overall thrust loss) associated with these devices must be within acceptable limits before they can be implemented in scramjet engines. The total pressure loss associated with recessed cavities is less than that of other flame holders that obstruct the flowfield. They are also attractive from a functional perspective because they can serve as integrated fuel-injection and flame-holding devices, which can hold stable flames over a wide range of operating conditions, as encountered in dual-mode scramjets. Cavities can be classified broadly as being acoustically open or closed, of which open-type cavities have been shown to have moderate drag penalty as compared with closed cavities [1]. In combustor systems, cavities have been shown to substantially increase the mixing rate and, in turn, the volumetric heat release [1]. Further, cavities with an inclined aft wall and cavities in tandem were shown to have efficient volumetric heat release [1,2]. In addition, direct cavity fuelling has proven to be more efficient than passive injection schemes in the recent past [3]. However, the direct fuelling technique may further complicate the process of controlling the cavity entrainment and may be undesirable from that perspective.

Numerous experiments have been carried out to study the effect of cavity geometric parameters, namely cavity length-to-depth ratio, offset ratio, and aft-wall angle and other parameters, such as injection pressure, injection location, passive and direct fuelling, and back pressure on the mixing and combustion characteristics of gaseous fuels like ethylene and hydrogen. In general, gaseous fuels, especially hydrogen, are preferred over liquid hydrocarbon fuels because evaporation of the fuel is not necessary and, in addition, their diffusivity is higher. However, for lower hypersonic flight regime ($M < 8$), which is of current interest, a liquid hydrocarbon fuel such as aviation kerosene is desirable owing to its high volumetric energy content and ease of handling. However, there are very few studies devoted to the understanding of fuel-air mixing and combustion phenomena of kerosene fuel. A brief review of the studies on the mixing and combustion characteristics of kerosene in the presence of cavities is presented next.

In a supersonic airstream, the effect of three different mixing schemes, namely rearward-facing step (baseline), modified rearward step with bevelled edges, and rearward-facing step along with a wedge placed downstream, on kerosene combustion was studied experimentally by Owens et al. [4]. Kerosene was injected downstream of the step in all the experiments, and the wedge was shown to enhance the mixing process. The rearward-facing step with bevelled edges yielded the maximum combustion efficiency due to vortex-enhanced mixing. Later, in the same configurations, the effect of air

Received 30 July 2008; revision received 4 November 2008; accepted for publication 4 November 2008. Copyright © 2008 by the American Institute of Aeronautics and Astronautics, Inc. All rights reserved. Copies of this paper may be made for personal or internal use, on condition that the copier pay the $10.00 per-copy fee to the Copyright Clearance Center, Inc., 222 Rosewood Drive, Danvers, MA 01923; include the code 0748-4658/09 $10.00 in correspondence with the CCC.

*Ph.D. Scholar, Department of Mechanical Engineering.
†Associate Professor; Department of Mechanical Engineering; vbabu@iitm.ac.in.

stagnation temperature, modulation of kerosene flow rate, and pilot hydrogen flow rate on flame stabilization were studied by injecting kerosene into the boundary layer upstream of the step [5]. At higher stagnation temperatures, preinjection of kerosene was shown to have a detrimental effect on flame stabilization. Further, modulation of the fuel flow rate resulted in minimal entrainment of core flow into the cavity, which resulted in a hydrogen-rich mixture inside the cavity and, hence, flame extinction. However, a reduction in the pilot hydrogen flow rate also resulted in flame extinction, in contrast to the finding of Vinogradov et al. [6].

The effect of kerosene spray without and with barbotage (using H_2) on the combustion characteristics in a model supersonic combustor was investigated by Gruenig and Mayinger [7]. Kerosene–H_2 mixture was shown to have better dispersion and produced fine droplets in the vicinity of the injector compared with a pure kerosene spray. Also, the mechanisms for self-ignition and combustion were studied at different combustor inlet air temperatures with hydrogen as well as kerosene. For hydrogen combustion, the self-ignition temperature was identified as the crucial parameter whereas for hydrocarbon combustion, self-ignition delay was shown to govern the combustion process. Furthermore, the fuel-specific combustion phenomena was explained through a gas dynamic feedback mechanism, which was reported to have a significant impact on kerosene combustion.

Similarly, Yu et al. [8] experimentally investigated the ignition and combustion characteristics of a pure kerosene spray along with pilot hydrogen in a model supersonic combustor. Various cavity module configurations with different pilot injection schemes were investigated. The fuel penetration and spreading rate was shown to increase by 30% with increase in injection pressure from 2.5 to 4.5 MPa. Cavity length and depth were shown to have a significant influence on the ignition and flame-holding characteristics. A local high temperature zone was shown to exist within the cavity, which assisted in flame-holding, and high combustion efficiency was achieved by using pilot hydrogen in conjunction with a recessed cavity configuration. Further, cavities in tandem were shown to be more effective in flame holding compared with a single cavity, requiring the lowest pilot hydrogen equivalence ratio. Later, the enhancement of stabilization and combustion using barbotaged (with air and H_2) kerosene was investigated [9] and compared with that of a pure kerosene spray. Barbotaging with hydrogen gas enhanced the combustion process by about 15–20%. However, this was influenced strongly by the conditions of effervescent atomization. Also, the injection location and scheme were shown to have a significant effect on the minimum pilot hydrogen equivalence ratio required for sustained combustion. In addition, vaporized kerosene was shown to have the potential of enhancing the fuel–air mixing [10]. Thus, supercritical (preheated) kerosene enhanced the combustion process by about 10–15% compared with pure kerosene, but the enhancement was marginal when compared with barbotaged kerosene.

Dufour and Bouchez [11] numerically investigated the combustion characteristics of kerosene injected from struts in a generic scramjet combustor. The predictions of wall static pressure profiles compared reasonably well with that of experimental data. Combustion efficiency was reported to be low due to the inefficient mixing of fuel and air. Numerical simulations of kerosene combustion in a dual-mode supersonic combustor were carried out by Rajasekaran and Babu [12]. Fuel was injected from wall-mounted injectors for the first stage and ramp based injectors for the second stage. The numerical calculations were able to predict the overall pressure rise reasonably well for both wall and ramp injection schemes. The over-prediction of pressure rise and heat release was attributed to the inadequacy of the single step chemistry to model complex hydrocarbon combustion.

Recently, Rajasekaran et al. [13] numerically investigated the effect of three different wall-mounted recessed cavity configurations on combustion characteristics of kerosene in a model supersonic combustor. Details of the flowfield, such as shocks, expansion fans, and flow separation inside the combustor, were predicted well. Further, the overall wall static pressure predictions were shown to agree reasonably well with experimental data. The success in predicting the overall pressure rise, which is crucial for designing a combustor, within acceptable limits in model combustors showed the capability of the numerical simulations for modelling kerosene combustion. This led Rajasekaran and Babu [14] to extend the numerical simulations to a full-scale concept combustor. In this study, from the baseline calculations, the ramp structure was shown to be very efficient for mixing. Further, based on preliminary results, the combustor design was improved by adjusting the location of ramps to enhance the lateral mixing and, in turn, the spread of heat release. Also, the wall divergence was increased to accommodate higher heat release. A CFD based design study for full-scale combustor designs has been reported recently by Manna et al [15]. They used the two-equation k-ϵ model for modelling turbulence. The eddy dissipation approach in conjunction with the mixed-is-burnt assumption was used for modelling the heat release and four strut-based combustor designs were investigated.

In all the preceding numerical simulations, the fuel injectors were modeled as surface injectors injecting droplets of constant diameter and the dispersion of the droplet trajectories due to the turbulent fluctuations of the continuous phase was ignored. These issues can be considered to be significant shortcomings from the injection modelling side. Also, the single-step chemistry can be identified as a major shortcoming from the chemical kinetics side. With these shortcomings in mind, the former issue has been addressed in this work by modelling the injection as a spray (which is more realistic), wherein the liquid fuel jet is disintegrated into fine droplets, and the droplet diameter is not constant but obeys a Rosin–Rammler distribution. This also increases the number and spread of the fuel streams and, in turn, the heat release. In the present work, the numerical simulations have been carried out to investigate the effect of the spray model on the mixing and combustion characteristics of kerosene in a model combustor with three different cavity configurations. The effect of injection pressure on the penetration of the fuel stream has been studied with different injection pressures. All the calculations have been performed using Fluent.

II. Computational Methodology

The supersonic model combustor considered in the present work is the same as the model experimentally studied by Yu et al. [8] and is shown in Fig. 1. It consists of three sections, a nearly constant area (section I) of length 0.266 m (with a 1 deg divergence for boundary-layer correction) followed by two expansion sections (II and III). The first expansion section (II) is 0.3 m long and has a 3 deg divergence, whereas the second expansion section (III) is 0.336 m long with 4 deg divergence. The section of the combustor is 0.0305×0.03 m at the entry and 0.07×0.03 m at the exit. The combustor has a detachable cavity module (to accommodate different cavity lengths and aft-wall angles) in section I. Three cavity configurations (named as models 1a, 1c, and 1d by Yu et al. [8]) of varying cavity lengths (45 and 61 mm) and aft-wall angles (15 and 45 deg) are studied in the present work. All the cavity configurations are the open type with a cavity module depth (denoted by h) of 8 mm. Kerosene fuel is injected at 300 K from five fuel-injection ports (each of 0.4 mm in diameter), located on the cavity ceiling and floor near the trailing edge of the cavity (at $5h$ in model 1a and $7h$ in models 1c and 1d from the cavity leading edge). Because all the present calculations have been carried out on a quarter geometry based on symmetry consideration, fuel is injected only from two and a half injection ports. The details of the three cavity configurations, and the

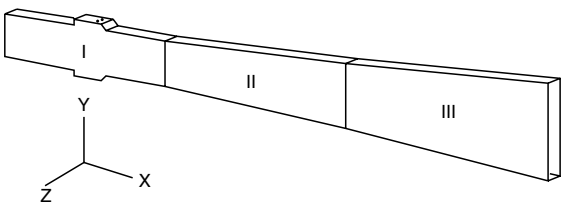

Fig. 1 Schematic of the model supersonic combustor [8].

Table 1 Combustor Details and Inlet Conditions

Model	Cavity length, m	Aft-wall angle	$T_{0,\text{inlet}}$, K	$P_{0,\text{inlet}}$, MPa	Equivalence ratio ϕ
1a	0.045	45 deg	1720	1.35	0.43
1c	0.061	15 deg	1730	1.30	0.44
1d	0.061	45 deg	1710	1.41	0.47

corresponding inlet stagnation conditions and equivalence ratio are given in Table 1.

Vitiated air (with the mass fractions of O_2, H_2O, and N_2 being 0.2, 0.134, and 0.666, respectively) enters the facility nozzle. The flow is accelerated to a nominal Mach number of 2.5 as it enters the combustor. The flow in the nozzle has also been simulated to capture the boundary layer on the walls accurately and to match the experimental combustor inlet conditions. In the simulations, three-dimensional, compressible, and turbulent Favre-averaged Navier–Stokes equations are solved along with the species conservation equation for the continuous phase. The calculations have been carried out primarily using the one-equation, Spalart–Allmaras (SA) model [16] but some calculations used the two-equation, SST (shear stress transport) k-ω model [17]. The motivation for using two different turbulence models is explained later. The SA model is a relatively simple and well-established model for aerospace applications, specifically for wall bounded flows. In this model, a separate transport equation for turbulent kinematic viscosity ν_t is solved. The SA model with default model constants ($C_{b1} = 0.1355$, $C_{b2} = 0.622$, $C_{v1} = 7.1$, $C_{w2} = 0.3$ $C_{w3} = 2.0$, and $\kappa = 0.4187$) has been used here. This model has been successfully used for modelling supersonic combustion of hydrogen [18]. The turbulent Schmidt number and Prandtl number are taken to be equal to 0.7 and 0.667, respectively. Sensitivity of the numerical predictions to the turbulent Schmidt number for ethylene [19] and hydrogen [20] fuel has been investigated already. The SST k-ω model is a hybrid of the standard k-ϵ and the k-ω models. This model is essentially a standard k-ω model near solid surfaces, which gradually switches to the standard high Reynolds number k-ϵ model away from solid surfaces. This feature combines the near-wall robustness of the k-ω turbulence model with the capabilities of the k-ϵ model away from the walls. It also includes the effect of turbulent shear stress transport based on Bradshaw's [21] assumption that the shear stress in a boundary layer is proportional to the turbulent kinetic energy. This modification improves the ability of this model to predict the flow separation better than the k-ϵ model. This model with default closure coefficients ($\alpha^*_\infty = 1$, $\alpha_\infty = 0.52$, $\beta^*_\infty = 0.09$, $R_\beta = 8$, and $\zeta^* = 1.5$) has been used in this study.

In an earlier investigation [13], the fuel injectors were modeled as surface injectors, wherein droplets are injected from each discretized face of the injector. Because the injector dimension is usually very small compared with the dimensions of the combustor, very fine meshing is necessary to have at least a few facets on the injection surface. The number of discretized faces varied from 6–8 for the various injectors [13]. Meshing the volume containing the injector face and blending it smoothly (i.e., with acceptable skewness of the cells) with the mesh in the surrounding volumes is usually a formidable task. Although it is possible to prescribe a distribution for the droplet diameter in the surface injection model, it is somewhat unrealistic to do so when the number of streams are so few. Hence, in the previous calculation using the surface injection model, the droplets were injected with a uniform diameter. This shortcoming was identified to result in excessive heat release locally and, thus, unreasonably high temperatures [13]. In the present work, this shortcoming and the difficulty with the meshing have been addressed by using a spray model.

Kerosene fuel is injected in the transverse direction (i.e., normal to the supersonic core flow) as a hollow cone spray (emanating from a simplex atomizer). The simplex atomizer model used here uses the linear instability sheet atomization (LISA) model proposed by Schmidt et al. [22]. In this model, the internal flowfield of the injector is not modeled separately as it is computationally too expensive for a three-dimensional calculation such as the present calculation and also due to the proprietary nature of the internal geometry details. Hence, a zero-dimensional model was used by Schmidt et al. [22] to represent the internal flowfield of the injector. A uniform velocity profile was assumed at the injector exit, and the velocity magnitude at the exit was related to the pressure difference a the injector.

Senecal et al. [23] showed that this model was able to predict the spray formation in both types of hollow cone sprays, namely, inwardly opening and outwardly opening atomizers, of which the former type is considered in the present work. The spray formation in this model is categorized into two stages 1) the film formation and 2) the sheet breakup and atomization process (Fig. 2). Senecal et al. [23] also showed that the effect of viscosity was minimal when the gas Weber number We_g is below 27/16 (critical Weber number We_{cr}), but in flow regimes where the $\text{We}_g > \text{We}_{\text{cr}}$ viscosity had to be considered to accurately predict the wave growth. However, in modern high-pressure fuel-injection systems, the velocities are high enough that the gas Weber number is above the critical limit. Nevertheless, in this spray model, the effect of liquid viscosity, surface tension, and the surrounding gas on the sheet breakup have been considered. After the sheet breakup, the ligament length can be calculated. This, in turn, allows the droplet diameter to be predicted. The actual size of the resulting droplet is chosen from a Rosin–Rammler distribution considering the predicted drop size as the mean size [23] with a spread parameter of 3.5, recommended by Schmidt et al. [24].

The input parameters for the spray model are the spray half angle, sheet constant, ligament constant, atomizer dispersion angle, and the azimuthal start and stop angle. In the present simulations, the spray half-angle is taken to be 30 deg based on spray visualization images by Yu et al. [25] for the case of liquid injection into a supersonic flow in the presence of a cavity. The sheet constant is taken to be 12 as recommended by Dombrowski and Hooper [26], who showed that this value predicted sheet breakup length, which agreed well with experimental sheet breakup lengths over a wide range of Weber numbers from 2 to 200. The ligament constant is taken as 0.5 as suggested by Schmidt et al. [22]. Sensitivity of the numerical predictions to the atomizer dispersion angle has been studied by running the calculations with two different dispersion angles, namely, 3.5 and 6 deg, and the results were found to be insensitive to the atomizer dispersion angle. Hence, a default dispersion angle of 6 deg has been used in all the simulations. A complete hollow cone spray from the periphery of the injection port is simulated by specifying the azimuthal start and stop angle as 0 and 360 deg.

The mass flow rate of fuel is calculated from the equivalence ratio. The fuel mass flow rate through each injection port is specified, and in each injection port the specified mass flow rate is assumed to be

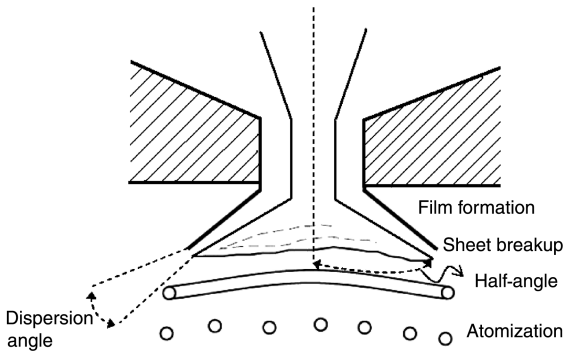

Fig. 2 Illustration of the hollow cone spray model, from Schmidt et al. [22].

distributed among 50 fuel streams based on past experience with gas turbine combustor simulations where 30 streams are customarily used. Because kerosene is injected in a liquid phase in the form of droplets, the simulations have been performed using a discrete-phase model. Here, in addition to solving the transport equations for the continuous phase, the discrete phase (dispersed in the continuous phase) is simulated in a Lagrangian frame of reference. Mass, momentum, and energy transfer between the two phases is accounted for in the simulations. The drag force on the dispersed droplets is calculated using the high Mach number law [27]. Dispersion of the droplets due to turbulence has been ignored in the calculations where the one-equation SA model was used for the continuous-phase turbulent flowfield, as it is not currently possible to model this effect with a one equation model. However, a two-equation model such as the SST k-ω model will allow this effect to be modeled. Hence, in order to evaluate the importance of the dispersion of the droplets due to turbulence, calculations using the SST k-ω model have also been carried out. In this case, the dispersive effect of the instantaneous velocity fluctuations of the turbulent continuous-phase flowfield on the droplet trajectory is accounted for using a stochastic tracking model. Droplet breakup, however, is not modeled.

Single-step, laminar finite rate kinetics has been used to model the chemistry. Rate data for the $C_{12}H_{23}$-O_2 forward reaction mechanism have been adapted from Westbrook and Dryer [28]. Viscosity and C_p of the mixture have been evaluated using a mass-weighted-mixing law. For the individual fluids in the mixture these properties have been evaluated using Sutherland's law and fifth-order polynomials in temperature, respectively.

A. Boundary Conditions

At the nozzle inlet, where the flow is subsonic, stagnation pressure, stagnation temperature, and species mass fractions are specified. In addition, inlet turbulence intensity (10%) and the hydraulic diameter (to estimate the turbulent length scale) have been specified. All the flow variables at the outlet boundary including pressure are determined from the interior of the domain by extrapolation, if the flow is supersonic. Otherwise, the exit pressure is taken to be equal to 100 kPa. All the walls are considered stationary, and standard wall functions have been used. Based on observations by Yu et al. [8] during their experiments, a constant wall temperature of 500 K has been specified. For the discrete phase, injection parameters, namely mass flow rate of kerosene, temperature, and upstream injection pressure, are specified. Also, the spatial location and the diameter of the injection ports are specified. In the SST k-ω model calculations, a two-way turbulence coupling is also enabled.

For combustor model 1a, a mixing study has been carried out with three injection pressures, namely 2.5, 3.5, and 4.5 MPa to study the effect of injection pressure on fuel mixing. Reacting flow calculations have been carried out only for 2.5 and 4.5 MPa injection pressures. Based on the results from combustor model 1a and in the absence of any information on the exact value for the injection pressure used in the experiments, the mixing and reacting flow calculations for combustor models 1c and 1d have been carried out with the injection pressure conservatively set to 2.5 MPa.

B. Grid Independence Study

For model 1a, calculations have been carried out using the same mesh as the one used by Rajasekaran et al. [13]. This mesh was obtained after grid adaption based on gradients of static pressure and species concentration to resolve the flow features and combustion phenomena accurately. In the case of models 1c and 1d, the domain has been remeshed, because remeshing the geometry improved the grid quality (i.e., in terms of wall y^+) with only a very modest increase in the overall cell count. However, considerable effort has been devoted to ensure that the cell count on the new meshes are very close to that of the old ones used by Rajasekaran et el. [13] so that the comparison of the predictions is fair. The grid size and the wall y^+ for all the models are given in Table 2. As pointed out by Rodriguez and Cutler [29], for turbulent calculations such as the present one, wall y^+ values less than 100 are generally acceptable, although lesser values are preferable. It is evident from Table 2 that the area-weighted average of wall y^+ for the three models is acceptable. In flows with shocks, it is very difficult to have low wall y^+ value throughout the domain. In the present calculations, the maximum value for wall y^+ given in Table 2 is seen near the separated flow region close to the combustor exit due to the imposed atmospheric pressure boundary condition at the exit. As this region is not of interest in the present context, further refinement in this region was deemed unnecessary.

Table 2 Grid refinement study for nonreacting and reacting flow calculations

Model	Number of cells	Maximum wall y^+	Average wall y^+
Nonreacting flow (without and with fuel injection)			
1a	649178	227	94
1c	766688	137	62
1d	750038	200	60
Reacting flow			
1a	649178	230	77
1c	766688	137	48
1d	750038	186	52

The accuracy of the solutions have been assessed through additional metrics such as global mass, momentum, and energy balance. For all the results reported here, the difference in mass flow rate between the inlet(s) and outlet is less than 1% of the injected fuel mass flow rate (fuel mass flow rate rather than the inlet mass flow rate is used because the former is two orders of magnitude less than the latter). The integrated value of the fuel mass flow rate for the nonreacting and reacting flow at various $x =$ constant sections downstream of the injection locations is within 4% of the injected fuel mass flow rate. This serves as a check on global fuel conservation and is also an important metric. Momentum balance has been checked by evaluating the left- and right-hand sides of the expression

$$\mathcal{F} = \left(\int p \mathrm{d}A + \int \rho u^2 \mathrm{d}A \right)_{\text{inlet}}^{\text{exit}}$$

separately and then calculating the difference. The right-hand side of this expression is the impulse function. The left-hand side is the net force acting on the walls (pressure + viscous) in the x direction. For all the results reported here, the difference between the left- and right-hand side of the preceding expression (for the continuous phase) is less than 5%. The overall energy balance is satisfied to within 5% of the inlet total enthalpy. All the calculations are second-order accurate.

III. Results and Discussion

In this section, predictions from nonreacting and reacting flow calculations are discussed for the three combustor configurations mentioned before. The combustion efficiency at different axial locations and the comparison of wall static pressure (along the combustor top wall) with the experimental values are also discussed.

A. Mixing Studies

In this section, the effect of the injection pressure on the droplet diameter distribution, Sauter mean diameter as well as the mixing efficiency is discussed. In addition, the effect of the dispersion of the droplets due to turbulence is also presented. Injection pressure can be expected to significantly influence the penetration and mixing (spreading and evaporation) of the liquid fuel droplets. The effect of the injection pressure is evaluated quantitatively using the evolution of the droplet diameter distribution and the mixing efficiency.

Figure 3 shows the histogram of the droplet diameter distribution on $x =$ constant planes located 25 mm, 50 mm, 75 mm, and 100 mm downstream of the injection location ($x = 0.235$ m) for 2.5 MPa injection pressure. These axial locations are in the region where most of the heat release takes place (i.e., within 100 mm downstream of the injection location). At $x = 0.26$ m, about 45% of the droplets have a

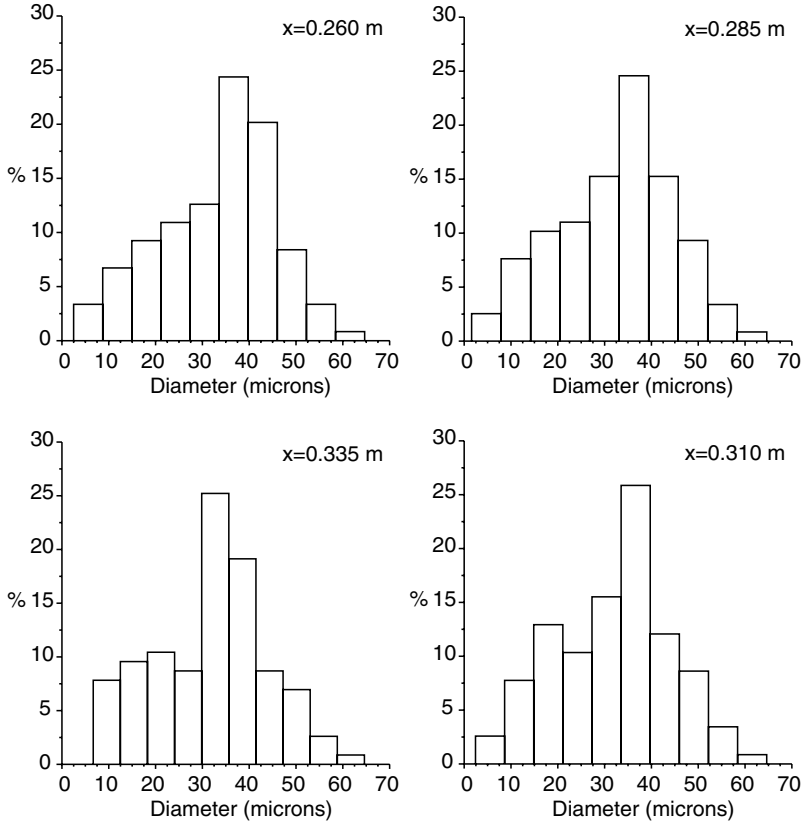

Fig. 3 Histogram of the droplet diameter distribution at different axial locations (clockwise from left top) for 2.5 MPa injection pressure (combustor model 1a).

diameter in between 35 and 45 μm. It can be seen that the droplet diameter decreases continuously along the axial distance, that is, at $x = 0.26$ m, almost 44% of the droplets have diameter less than 35 μm, whereas at $x = 0.335$ m the percentage increases to 60%. This trend is more prominent with increase in injection pressure. In the first three axial locations, the highest percentage of droplets are shown to be in between 35 and 45 μm. However, at $x = 0.335$ m, the maximum percentage of droplets are between 30 and 35 μm. This, in turn, gives an indication of the evaporation time (or distance) scale. The decrease in droplet diameter is more rapid at the higher injection pressure due to the higher penetration of the fuel spray into the flow. This increased penetration can be expected to result in an increase of heat release in the core region as opposed to the earlier cases [13,14], where the heat release occurred near the top wall. This is due to the fact that, in the surface injection model, all the droplets had a diameter equal to 20 μm at the injection location itself. In contrast, in the present study, it can be seen from Fig. 3 that only 10% of the droplets have a diameter close to this value near the injection location.

Axial variation of the Sauter mean diameter (SMD), for three injection pressures, from just downstream of the injection location until the combustor exit are shown in Fig. 4. The SMD (which characterizes the entire spray) at any location decreases with an increase in injection pressure. The smaller droplet diameter in conjunction with increased penetration and spreading that is seen at higher injection pressures can be expected to result in higher mixing and combustion efficiencies. The reduction in SMD value due to an increase in injection pressure from 2.5 to 3.5 MPa is more than that due to an increase from 3.5 to 4.5 MPa. In the region ($0.235 < x < 0.335$ m) where much of the heat release takes place, the SMD is close to 32 and 30 μm for injection pressures 3.5 and 4.5 MPa, respectively. At the combustor exit, about 72, 90, and 94% of the droplets have diameters less than 30 μm for 2.5, 3.5, and 4.5 MPa injection pressure, respectively. This clearly highlights the effect of injection pressure on the droplet evaporation for the nonreacting case. In the reacting flow case, the SMD values

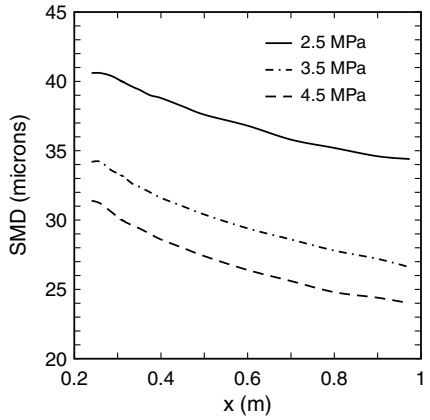

Fig. 4 Axial variation of the SMD for three injection pressures using SA model (combustor model 1a).

immediately downstream of the injection location are of more interest and importance because smaller droplets will evaporate and mix faster, resulting in higher combustion efficiency. Yu et al. [8] reported a 5 μm decrease in mean droplet diameter size when the injection pressure was increased from 2.1 to 4.5 MPa. However, the present study shows a 10 μm change in SMD immediately downstream of the injection location for approximately the same range of injection pressure.

Figure 5 shows the penetration of fuel streams injected (at 2.5 and 4.5 MPa) from the cavity ceiling into the flow in combustor model 1a. It can be seen from Fig. 5 that the penetration of the spray into the flow is less at an injection pressure of 2.5 MPa. Consequently, most of the droplet streams impact the slant aft-wall of the cavity and are deflected towards the bottom symmetry plane. Whereas, at an injection pressure of 4.5 MPa, the penetration of the fuel streams into the flow is higher, which, in turn, results in a smaller number of fuel

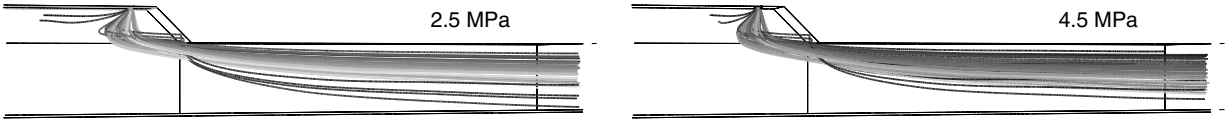

Fig. 5 Penetration of fuel streams injected at 2.5 MPa (left) and 4.5 MPa (right) into the flow in combustor model 1a.

streams colliding with the cavity slant wall. Moreover, some of the injected fuel streams are trapped in the recirculation region inside the cavity, and these are seen moving upstream of the injection location in Fig. 5. This will result in marginal heat release and a rise in wall static pressure ahead of the injection location. Yu et al. [8] reported that there was a 30% increase in the penetration and spreading of the spray with increase in the injection pressure from 2.5 to 4.5 MPa, based on the visualization of the spray (in the absence of a cavity). Although the experimental visualization was done without the cavity, the predicted change in the penetration of fuel streams with the injection pressure by the present calculations is consistent with the experimental observation.

Mixing efficiency, in addition to SMD, is also evaluated in the present work to quantify the effect of injection pressure. Here, mixing efficiency at any $x =$ constant plane is defined as [30]

$$\eta_m = \frac{\int_x \alpha_R \rho u \mathrm{d}A}{\sum_x \dot{m}_{\mathrm{fuel,in}}}$$

The denominator represents the total amount of fuel injected upstream of this section. The quantity α_R in the numerator is given as [30]

$$\alpha_R = \begin{cases} \alpha & \alpha \le \alpha_s \\ \alpha_s \frac{1-\alpha}{1-\alpha_s} & \alpha > \alpha_s \end{cases}$$

where α is the actual fuel mass fraction, α_s is the stoichiometric fuel mass fraction corresponding to the oxygen mass fraction at that location, ρ is the density, u is the axial velocity, and $\dot{m}_{\mathrm{fuel,in}}$ is the mass flow rate of fuel injected upstream of this plane. Mixing efficiency is thus a measure of the percentage of the fuel that is likely to burn under stoichiometric conditions.

Variation of mixing efficiency for three injection pressures for combustor model 1a is shown in Fig. 6. Mixing efficiency is seen to increase with injection pressure. There is a 20% increase in the mixing efficiency at the combustor exit between the lowest and the highest injection pressure. For a liquid fuel such as kerosene, combustion can take place only after evaporation and mixing has taken place, unlike a gaseous fuel. Higher mixing efficiency is thus essential, because the available combustor length is fixed. The highest mixing efficiency in the present case is only about 79%, which is considerably lower than the corresponding value for a gaseous fuel such as hydrogen [18] or ethylene [30]. Furthermore, the mixing efficiency in the cavity and immediately downstream, where combustion is likely to take place, is less than 50% (Fig. 6). Consequently, combustion efficiency will also likely be lower.

Dispersion of the droplets due to the turbulence field can be expected to enhance mixing. Figure 7 shows the effect of turbulent dispersion on the mixing efficiency in combustor model 1a at 2.5 MPa injection pressure. Because the turbulence model had to be changed to enable the modelling of the dispersion of the droplets, the change in mixing efficiency due to the change in turbulence model alone (i.e., in the absence of turbulent dispersion) has to be ascertained first. Earlier investigations in model combustors [13,18,31] have shown that the SA model overpredicts mixing. Likewise, in the present work the SA model predicts higher mixing efficiency when compared with the SST k-ω model prediction. However, the maximum difference in the mixing efficiency predicted by these models is only about 5%. When the effect of turbulent dispersion is also included, the mixing efficiency predicted by the SST k-ω model is higher and is more than the SA model prediction. In the region $0.235 < x < 0.335$ m, where much of the heat release ultimately takes place, the difference in the mixing efficiency predicted by the SA model and SST k-ω model with turbulent dispersion is very minimal. However, the difference in the mixing efficiency predicted using the SST k-ω model without and with turbulent dispersion is significant even in the region of heat release as can be seen in Fig. 7. This highlights the fact that the dispersion of the droplets augments the mixing considerably and this can be expected to have a significant influence on the heat release. As mentioned earlier, the importance of the mixing study for a liquid fuel such as kerosene lies in the fact that evaporation has to take place first followed by mixing and then combustion. This adds another time delay to the heat release process.

B. Combustion Studies

In this section, results from reacting flow calculations for the three combustor models are discussed. Contours of dimensionless heat release and axial velocity are presented and discussed for combustor model 1a. The combustion efficiency for all the combustor models are discussed next.

Figure 8 shows the contours of dimensionless heat release and axial velocity (m/s) at different axial locations inside the cavity and immediately downstream of the cavity in combustor model 1a. The dimensionless heat release at a location is defined as the increase in the stagnation temperature at that location over the value at the inlet and nondimensionalized using the inlet stagnation temperature. In Fig. 8, the cross section of the separated flow region on the side wall due to the pressure rise accompanying the heat release in the cavity is

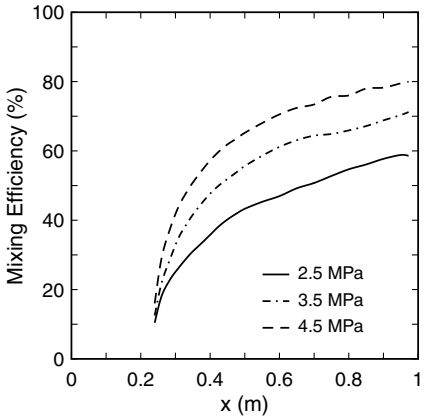

Fig. 6 Effect of injection pressure on mixing efficiency for combustor model 1a.

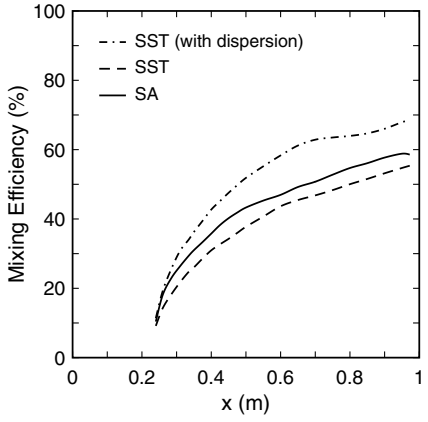

Fig. 7 Effect of turbulent dispersion on mixing efficiency.

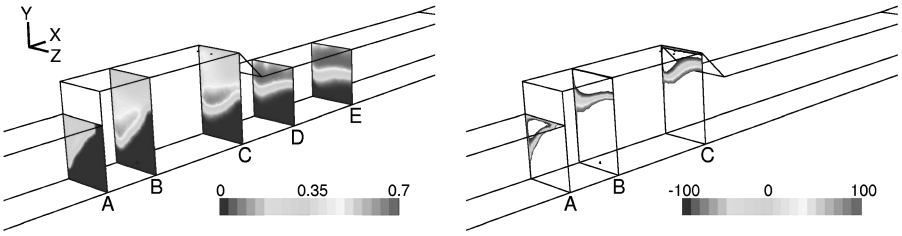

Fig. 8 Contours of dimensionless heat release (left) and axial velocity (right) in combustor model 1a.

shown in plane A. It is evident that the heat release in plane A is confined within the separated flow region. In planes B and C, the region at which the axial velocity changes from 100 to −100 m/s is shown as the approximate location of the shear layer. Inside the cavity, some of the fuel streams are trapped inside the recirculation zone due to which heat release occurs upstream of the injection location. However, most of the heat release occurs at the periphery of the recirculation region/shear region and outside the cavity volume, that is, in the central part of the cross section as shown in planes B and C in Fig. 8. Also, the considerable amount of heat release inside the cavity acts a constant ignition source and flame holding, which is consistent with the experimental finding by Yu et al. [8] Further downstream in plane D, the heat release occurs near the top wall owing to the tendency of the particle trajectories to stay close to the top wall (Fig. 5). This, in turn, highlights the fact that the heat release downstream of the injection location is controlled by the penetration of the fuel streams in the domain. Heat release is essentially complete by the end of section I, as there is not much change in the heat release contours between planes D and E. This correlates well with the mixing efficiency curve in Fig. 7, where the gradient is very steep from the injection location up to $x = 0.45$ m, suggesting that the heat release in this region is likely mixing controlled. Further downstream (i.e., $0.45 \leq x \leq 0.6$ m) the gradient is less steep indicating that the mixing levels are off. It may be inferred then that mixing may not play a dominant role any more and that the heat release in this region may be determined by both the mixing and the kinetics.

Combustion efficiency is one of the key performance metrics used to evaluate a combustor. In this study, the combustion efficiency is calculated based on the fuel consumption at any given $x =$ constant plane. Hence, it gives an indication of the completeness of the combustion process. Combustion efficiency on a given $x =$ constant plane is given as [30]

$$\eta_c = \frac{\int_x \frac{167}{12\times 44}\alpha\rho u \mathrm{d}A}{\sum\limits_x \dot{m}_{\mathrm{fuel,in}}}$$

where α is the mass fraction of CO_2 and the multiplicative constant in the numerator accounts for the fact that 12 kmoles (12×44 kg) of CO_2 are produced from the combustion of 1 kmole (167 kg) of fuel.

Figure 9 shows the variation of combustion efficiency for combustor model 1a. The combustion efficiencies calculated for the lowest (2.5 MPa) and the highest (4.5 MPa) injection pressure using the spray model are compared with that of the surface injection [13] model. As discussed earlier, the combustion efficiency for the 4.5 MPa injection pressure is higher than that of the 2.5 MPa injection pressure, on account of the higher mixing efficiency in the former case. This also highlights the fact that the smaller droplets (as a result of higher injection pressure) burn faster even at supersonic speeds. The combustion efficiency values predicted using the spray model are lower than that of the surface injection model but are more realistic. In all the cases, almost 90% of the fuel consumption takes place within $x \simeq 0.4$ m, beyond which the combustion efficiency curves remain almost flat. This is consistent with the experimental trend, where the maximum pressure rise occurs within 0.15 m downstream of the injection location.

Figure 10 shows the comparison of combustion efficiency predicted using the SA model with that of the SST k-ω model without and with turbulent dispersion at 2.5 MPa injection pressure for combustor model 1a. The combustion efficiency calculated using the

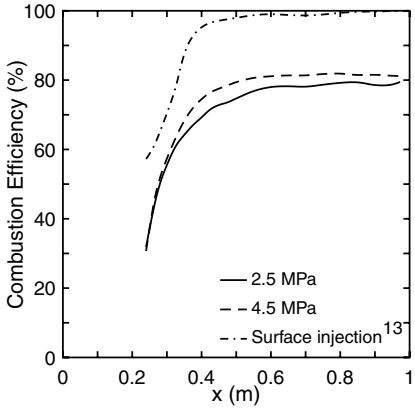

Fig. 9 Comparison of combustion efficiency for different injection schemes and injection pressures for combustor model 1a.

SST k-ω model with turbulent dispersion is the highest and consistent with the mixing efficiency prediction. The combustion efficiencies calculated using the SA model and the SST k-ω model without turbulent dispersion are almost the same, although the mixing efficiencies are different. It can be seen from Fig. 10 that the effect of turbulent dispersion is significant along the entire combustor length.

Variation of combustion efficiency for combustor models 1c and 1d obtained using the spray model and the surface injection model [13] are shown in Fig. 11. The use of the smaller and constant value for the droplet diameter in the surface injection model results in the combustion efficiency reaching 100%. In contrast, the spray model predicts more realistic maximum values for the combustion efficiency. When using the spray model, combustor model 1d shows the highest combustion efficiency, namely 85%. This could be due to the fact that, of the three combustor models studied, this model has the largest cavity volume. Furthermore, when the surface injection model is used, the combustion efficiency for both of these models is almost the same, whereas with the spray model they are reasonably different.

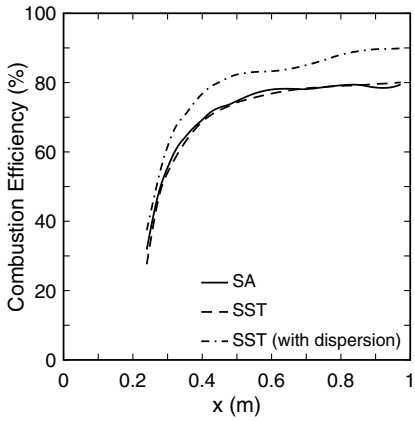

Fig. 10 Comparison of combustion efficiency using SA model and SST k-ω model without and with turbulent dispersion at 2.5 MPa injection pressure for combustor model 1a.

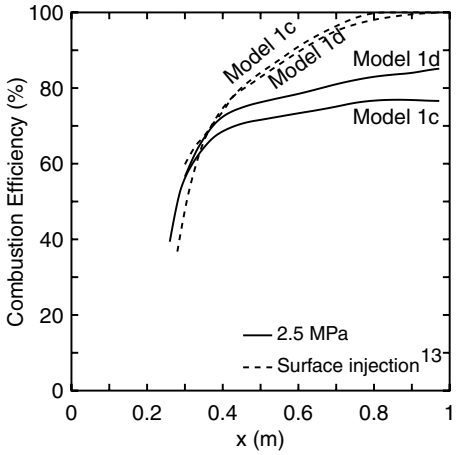

Fig. 11 Comparison of combustion efficiency using spray and surface injection schemes for combustor models 1c and 1d.

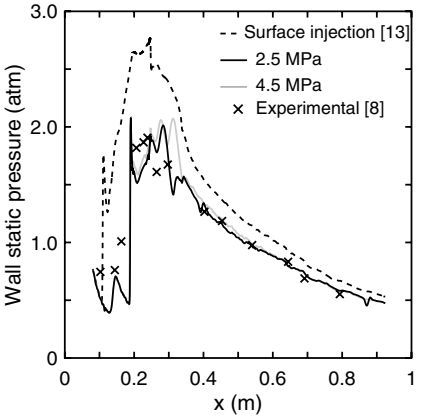

Fig. 12 Comparison of wall static pressure predictions using spray and surface injection model [13] with the experimental data [8] for combustor model 1a.

As discussed earlier, the heat release in the section between the injection location and $x \approx 0.45$ m is mixing dominated for combustor model 1a (and indeed for models 1c and 1d as well). Figures 9–11 show that the combustion efficiency curves for all the model combustors are steep in this section, then gradually level off and become flat beyond $x = 0.6$ m. This indicates that the chemical reaction and, hence, the heat release tapers off beyond $x = 0.6$ m. Because the flow expands and accelerates in this part of the combustor, the static temperature and the reaction rate decrease quite rapidly, and the flow is essentially chemically frozen beyond $x = 0.6$ m. It can be concluded that the heat release in the region $0.45 \leq x \leq 0.6$ m is controlled by mixing and kinetics, with the kinetic time scale gradually becoming longer as the reaction rate decreases. The preceding results clearly bring out the fact that for a liquid fuel such as kerosene, the regions and the amount of heat release strongly depend on the extent of mixing of the fuel with the flow. Such intricate details are captured better with a spray model, wherein a higher number of fuel streams are allowed to spread over a larger volume as opposed to the surface injection model.

C. Comparison with Experimental Data

Wall static pressure on the top wall from the numerical calculations and the experiments [8] for all the combustor models are given in Figs. 12–15. Figure 12 shows the comparison of wall static pressure obtained using the spray model for two injection pressures, namely 2.5 and 4.5 MPa with the experimental data for combustor model 1a. With the spray model, the wall static pressure predictions remain almost the same everywhere, despite the increase in injection pressure, except for the additional peak predicted at $x \approx 0.325$ m with the higher injection pressure. Beyond $x = 0.4$ m, the static pressure predicted by the spray model is well within the uncertainty in the experimental measurements.

Figure 13 shows the comparison of wall static pressure prediction using the SA model and the SST k-ω model (without and with turbulent dispersion) with the experimental data for combustor model 1a. The wall static pressure predictions using the SA model and the SST k-ω model without turbulent dispersion are almost the same. However, the peak pressure values predicted using the SST k-ω model with turbulent dispersion are higher than the other predictions. The location of the initial pressure rise closer to the cavity front wall region is predicted to be marginally upstream compared with the other two model predictions. In the cavity region, the first two pressure peaks are predicted better by including the dispersion effect. Also, these calculations predict the pressure rise to be spread out, that is, the profile exhibits a plateau rather than a peak. Beyond $x = 0.4$ m, the wall static pressure prediction using the SST k-ω model with turbulent dispersion is marginally higher than the experimental data. This is likely due to the predictions of the mixing efficiency and, in turn, the combustion efficiency being higher along the entire combustor length when dispersion is taken into account.

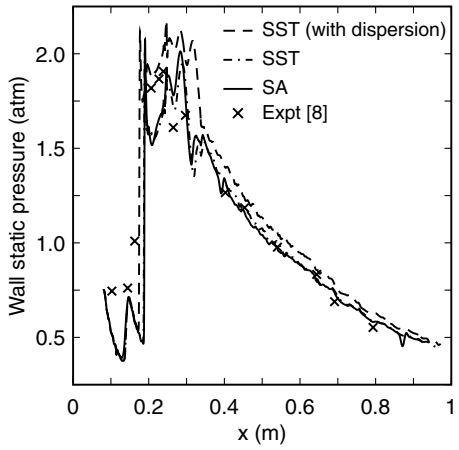

Fig. 13 Comparison of wall static pressure predictions using the SA model and the SST k-ω model (without and with turbulent dispersion) with experimental data [8] at 2.5 MPa injection pressure for combustor model 1a.

Figure 14 shows the comparison of wall static pressure predicted using the spray and the surface injection model with the experimental data for combustor model 1c. In this model, the cavity length is more than in model 1a whereas the aft-wall inclination is less than that of model 1a. The pressure rise in the cavity region is underpredicted somewhat by the present calculation. A higher value for the injection pressure or inclusion of the turbulent dispersion of the droplets in the reacting flow calculations or a better chemistry model may improve the prediction in this region. However, at $x \simeq 0.3$ m the wall static pressure prediction is shown to agree well with the experimental data. This is due to the fact that with a smaller inclination of the aft wall, the fuel streams move closer to the top wall immediately downstream of the injection location, which results in heat release close to the top wall. The agreement between the predictions and the experiment beyond $x = 0.4$ m is within 5%. The reason for the anomalous trend in the experimental data at $x \simeq 0.6$ m is not clear.

Figure 15 shows the comparison of wall static pressure predicted using the spray and surface injection model with the experimental data for combustor model 1d. In this model, the cavity length is the same as that of model 1c whereas the aft-wall inclination is same as in model 1a. The increase in the aft-wall inclination assists in the penetration of the fuel into the flow. Further, with increase in cavity length the cavity volume is increased, which, in turn, results in more heat release inside the cavity. This is captured quite well by the present calculations using the spray model. In this case also, the predictions are within 5% of the experimental values.

From all the preceding results, it can be clearly seen that predictions using the spray model are superior to the earlier

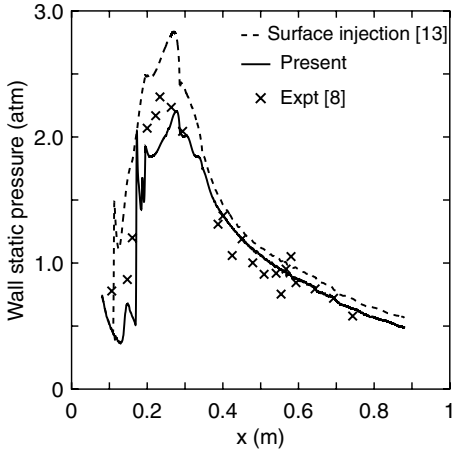

Fig. 14 Comparison of wall static pressure predictions using spray and surface injection model [13] with the experimental data [8] for combustor model 1c.

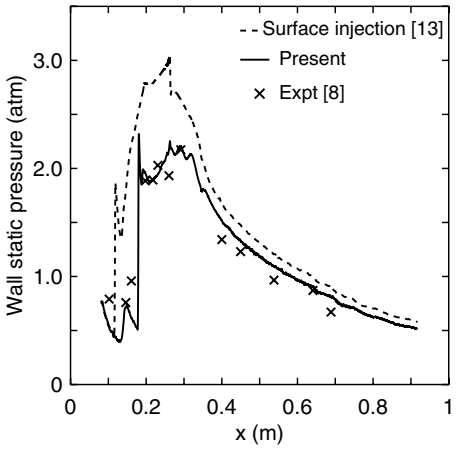

Fig. 15 Comparison of wall static pressure predictions using spray and surface injection model [13] with the experimental data [8] for combustor model 1d.

predictions using the surface injection model [13], wherein the pressure rise was overpredicted consistently. The location of the pressure rise, the peak value, and the overall trend predicted by the present calculations agree with the experimental data to within 5% for combustor models 1a and 1d and within 10% for combustor model 1c. It is interesting to note that the predictions using the spray and surface injection model differ significantly only in section I of the combustor where heat release takes place and they are reasonably close beyond $x = 0.4$ m (i.e., sections I and II).

IV. Conclusions

Results from the nonreacting and reacting flow calculations in three model combustors with kerosene fuel have been presented. Earlier investigations on the supersonic combustion of hydrogen [18] and kerosene [13] fuels have shown that mixing of the fuel with the supersonic flow plays an important role in the heat release, and, in turn, thrust generation in supersonic combustors. This is especially true for a liquid fuel such as kerosene, because the evaporation of the fuel has to take place before mixing, and the evaporation time adds to the time delay in the heat release process. In the present work, the fuel injection is modeled using a hollow cone spray model in contrast to the earlier calculations that used a surface injection model. With the spray model, the fuel streams are shown to spread over a larger volume than before. It is shown that the penetration and spreading of the fuel as well as the rate of decrease of droplet diameter increase with an increase in the injection pressure. The mixing efficiency also increases with increasing injection pressure. The effect of turbulent dispersion on the droplets is shown to be significant in the region of heat release and further downstream.

Contours of the dimensionless stagnation temperature together with the mixing efficiency have been used to clearly draw insights on the nature of the heat release. With the spray model, the fuel streams penetrate more into the core flow. Consequently, the heat release in the cavity occurs in the region where the mixing and kinetic time scales are of the same order. Further downstream, in the diverging section where the flow is expanding, the heat release is kinetically controlled, due both to the increasing velocity and the decreasing temperature, which, in turn, lowers the reaction rate. The combustion efficiency is seen to increase with an increase in the injection pressure, owing to higher mixing efficiency. Although the combustion efficiencies calculated with the spray model are lower than that of the surface injection model, they are more realistic. Of the three combustor models studied, the combustion efficiency is the highest for model 1d, owing to higher cavity volume and consequently higher heat release.

In all the combustor models, the comparison of wall static pressure predicted using the spray injection model with the experimental data [8] is seen to be superior to the earlier predictions using the surface injection model. In all the cases, both peak values and the locations are predicted to within 5% of the experimental value, despite the use of a single-step chemistry model. However, in combustor model 1c, the pressure rise in the cavity region is somewhat underpredicted by the present calculation. It may be worth investigating to see whether the predictions can be improved for model 1c by including the dispersive effect on the droplets, for the reasons mentioned earlier in connection with the heat release. The present calculations clearly demonstrate that the predictions of model combustors operating with low equivalence ratios, the global reaction assumption is adequate. However, scaling the predictions to a full-scale combustor and higher equivalence ratios may demand a detailed chemistry model (especially in the kinetically controlled regions) in view of the fact that heat release is higher with a detailed chemistry model [32].

Acknowledgments

The authors would like to thank S. Panneerselvam and V. Ramanujachari of the Defence Research and Development Laboratory in Hyderabad, India for providing financial support for this work through a grant. The authors gratefully acknowledge the insightful comments and suggestions given by the reviewers.

References

[1] Yu, K. H., Wilson, K. J., and Schadow, K. C., "Effect of Flame-Holding Cavities on Supersonic-Combustion Performance," *Journal of Propulsion and Power*, Vol. 17, No. 6, 2001, pp. 1287–1295. doi:10.2514/2.5877

[2] Ben-Yakar, A., and Hanson, R. K., "Cavity Flame-Holders for Ignition and Flame Stabilization in Scramjets: An Overview," *Journal of Propulsion and Power*, Vol. 17, No. 4, 2001, pp. 869–877. doi:10.2514/2.5818

[3] Rasmussen, C. C., Driscoll, J. F., Hsu, K.-Y., Donbar, J. M., Gruber, M. R., and Carter, C. D., "Stability Limits of Cavity-Stabilized Flames in Supersonic Flow," *Proceedings of the Combustion Institute*, Vol. 30, No. 2, 2005, pp. 2825–2833. doi:10.1016/j.proci.2004.08.185

[4] Owens, M. G., Segal, C., and Auslender, A. H., "Effects of Mixing Schemes on Kerosene Combustion in a Supersonic Airstream," *Journal of Propulsion and Power*, Vol. 13, No. 4, 1997, pp. 525–531. doi:10.2514/2.5198

[5] Owens, M. G., Tehranian, S., Segal, C., and Vinogradov, V. A., "Flame-Holding Configurations for Kerosene Combustion in a Mach 1.8 Airflow," *Journal of Propulsion and Power*, Vol. 14, No. 4, 1998, pp. 456–461. doi:10.2514/2.5322

[6] Vinogradov, V. A., Kobigsky, S. A., and Petrov, M. D., "Experimental Investigation of Kerosene Fuel Combustion in Supersonic Flow," *Journal of Propulsion and Power*, Vol. 11, No. 1, 1995, pp. 130–134. doi:10.2514/3.23850

[7] Gruenig, C., and Mayinger, F., "Supersonic Combustion of Kerosene/H_2 Mixtures in a Model Scramjet Combustor," *Combustion Science*

and Technology, Vol. 146, No. 1, 1999, pp. 1–22.
doi:10.1080/00102209908924205

[8] Yu, G., Li, J. G., Chang, X. Y., Chen, L. H., and Sung, C. J., "Investigation of Kerosene Combustion Characteristics with Pilot Hydrogen in Model Supersonic Combustor," *Journal of Propulsion and Power*, Vol. 17, No. 6, 2001, pp. 1263–1272.
doi:10.2514/2.5874

[9] Yu, G., Li, J. G., Chang, X. Y., Chen, L. H., and Sung, C. J., "Fuel Injection and Flame Stabilization in a Liquid-Kerosene-Fueled Supersonic Combustor," *Journal of Propulsion and Power*, Vol. 19, No. 5, 2003, pp. 885–893.
doi:10.2514/2.6179

[10] Fan, X., Yu, G., Li, J. G., Zhang, X. Y., Chen, L. H., and Sung, C. J., "Investigation of Vaporized Kerosene Injection and Combustion in a Supersonic Model Combustor," *Journal of Propulsion and Power*, Vol. 22, No. 1, 2006, pp. 103–110.
doi:10.2514/1.15427

[11] Dufour, E., and Bouchez, M., "Computational Analysis of a Kerosene-Fuelled Scramjet," AIAA Paper 01-1817, 2001.

[12] Rajasekaran, A., and Babu, V., "Numerical Simulation of Kerosene Combustion in a Dual Mode Supersonic Combustor," AIAA Paper 06-5041, 2006.

[13] Rajasekaran, A., Satish Kumar, G., and Babu, V., "Numerical Simulation of the Supersonic Combustion of Kerosene in a Model Combustor," *Progress in Computational Fluid Dynamics* (to be published).

[14] Rajasekaran, A., and Babu, V., "Evaluation of a Ramp Cavity Based Concept Supersonic Combustor using CFD," *Progress in Computational Fluid Dynamics*, (to be published).

[15] Manna, P., Behera, R., and Chakraborty, D., "Liquid-Fueled Strut-Based Scramjet Combustor Design: A Computational Fluid Dynamics Approach," *Journal of Propulsion and Power*, Vol. 24, No. 2, 2008, pp. 274–281.
doi:10.2514/1.28333

[16] Spalart, P. R., and Allmaras, S. R., "A One-Equation Turbulence Model for Aerodynamic flows," AIAA Paper 92-0439, 1992.

[17] Menter, F. R., "Zonal Two Equation k-ω Models for Aerodynamic Flows," AIAA Paper 93-2906, 1993.

[18] Rajasekaran, A., and Babu, V., "Numerical Simulation of Three-Dimensional Reacting Flow in a Model Supersonic Combustor," *Journal of Propulsion and Power*, Vol. 22, No. 4, 2006, pp. 820–827.
doi:10.2514/1.14952

[19] Baurle, R. A., and Eklund, D. R., "Analysis of Dual-Mode Hydrocarbon Scramjet Operation at Mach 4-6.5," *Journal of Propulsion and Power*, Vol. 18, No. 5, 2002, pp. 990–1002.
doi:10.2514/2.6047

[20] Rajasekaran, A., and Babu, V., "On the Effect of Schmidt and Prandtl Numbers in the Numerical Predictions of Supersonic Combustion," AIAA Paper 06-5037, 2006.

[21] Bradshaw, P., Ferriss, D. H., and Atwell, N. P., "Calculation of Boundary-Layer Development Using the Turbulent Energy Equation," *Journal of Fluid Mechanics*, Vol. 28, No. 3, 1967, pp. 593–616.
doi:10.1017/S0022112067002319

[22] Schmidt, D. P., Nouar, I., Senecal, P. K., Rutland, C. J., Martin, J. K., Reitz, R. D., and Hoffman, J. A., "Pressure-Swirl Atomization in the Near Field," Society of Automotive Engineers Paper SAE 01-0496, 1999.

[23] Senecal, P. K., Schmidt, D. P., Nouar, I., Rutland, C. J., Reitz, R. D., and Corradini, M. L., "Modeling High-Speed Viscous Liquid Sheet Atomization," *International Journal of Multiphase Flow*, Vol. 25, No. 6, 1999, pp. 1073–1097.
doi:10.1016/S0301-9322(99)00057-9

[24] Schmidt, D. P., Corradini, M. L., and Rutland, C. J., "A Two-Dimensional, Non-Equilibrium Model of Flashing Nozzle Flow," *3rd ASME/JSME Joint Fluids Engineering Conference*, American Society of Mechanical Engineers, Paper FEDSM99-7856, 1999.

[25] Yu, G., Li, J. G., Yang, S. R., Yue, L. J., Zhang, X. Y., Huang, Y., and Sung, C. J., "Investigation of Liquid Hydrocarbon Combustion in Supersonic Flow Using Effervescent Atomization," AIAA Paper 02-4279, 2002.

[26] Dombrowski, N., and Hooper, P. C., "The Effect of Ambient Density on Drop Formation in Sprays," *Chemical Engineering Science*, Vol. 17, No. 4, 1962, pp. 291–305.
doi:10.1016/0009-2509(62)85008-8

[27] Clift, R., Grace, J. R., and Weber, M. E., *Bubbles, Drops, and Particles*, Academic Press, New York, 1978.

[28] Westbrook, C. K., and Dryer, F. L., "Chemical Kinetic Modeling of Hydrocarbon Combustion," *Progress in Energy and Combustion Science*, Vol. 10, No. 1, 1984, pp. 1–57.
doi:10.1016/0360-1285(84)90118-7

[29] Rodriguez, C. G., and Cutler, A. D., "Numerical Analysis of the SCHOLAR Supersonic Combustor," NASA CR-2003-212689, Dec. 2003.

[30] Baurle, R. A., Mathur, T., Gruber, M. R., and Jackson, K. R., "A Numerical and Experimental Investigation of a Scramjet Combustor for Hypersonic Missile Applications," AIAA Paper 98-3121, 1998.

[31] Kumaran, K., Rajasekaran, A., and Babu, V., "A Comparison of Numerical Predictions of the Supersonic Combustion of Hydrogen using S-A and SST k-ω Models," *Progress in Computational Fluid Dynamics* (submitted for publication).

[32] Kumaran, K., and Babu, V., "Investigation of the Effect of Chemistry Models on the Numerical Predictions of the Supersonic Combustion of Hydrogen," *Combustion and Flame* (submitted for publication).

J. Oefelein
Associate Editor